Chinese Chemical Letters 34 (2023) 108711

Contents lists available at ScienceDirect

Chinese Chemical Letters

journal homepage: www.elsevier.com/locate/cclet

Gel electrolyte *via in situ* polymerization to promote durable lithium-air batteries

Renfei Cao [a,1], Kai Chen [b,1], Yangfeng Cui [a], Jianwei Liu [b], Wanqiang Liu [a,*], Gang Huang [b,*], Xinbo Zhang [b,*]

[a] School of Materials Science and Engineering, Changchun University of Science and Technology, Changchun 130022, China
[b] State Key Laboratory of Rare Earth Resource Utilization, Changchun Institution of Applied Chemistry, Chinese of Academy of Sciences, Changchun 130022, China

ARTICLE INFO

Article history:
Received 17 May 2023
Revised 9 June 2023
Accepted 19 June 2023
Available online 25 June 2023

Keywords:
In situ polymerization
Gel electrolyte
Gradient sei film
Lithium anode
Lithium-air batteries

ABSTRACT

Aprotic lithium-air batteries (LABs) have been known as the holy grail of energy storage systems due to their extremely high energy density. However, their real-world application is still hindered by the great challenges from the Li anode side, like dendrite growth and corrosion reactions, thus a pure oxygen atmosphere is usually adopted to prolong the lifetime of LABs, which is a major obstacle to fully liberate the energy density advantages of LABs. Here, a gel polymer electrolyte has been designed through *in-situ* polymerization of 1,3-dioxolane (DOL) by utilizing the unique semi-open nature of LABs to protect the Li anode to conquer its shortcomings, enabling the high-performance running of LABs in the ambient air. Unlike common liquid electrolytes, the *in-situ* formed gel polymer electrolyte could facilitate constructing a gradient SEI film with the gradual decrease of organic components from top to bottom, preventing the Li anode from dendrite growth and air-induced corrosion reactions and thus realizing durable Li repeated plating/stripping (2000 h). Benefiting from the anode protection effects of the gradient SEI film, the LABs display a long lifetime of 170 cycles, paving an avenue for practical, long-term, and high-efficiency operation of LABs.

The demands for high-efficiency utilization of renewable energy sources and reduction of carbon dioxide emission have been growing rapidly since the proposal of carbon neutrality targets in China. Battery technologies are promising systems to store renewable energy to reduce our dependence on traditional energy sources in the power generation and transportation areas [1,2]. However, the energy density of commercial lithium-ion batteries (LIBs) is still far lower than that of fossil fuels and cannot meet the long cruising range requirement of electric vehicles. Therefore, developing new battery systems with high specific energy densities has become an inevitable choice [3–5]. Among the available battery technologies, lithium-air batteries (LABs) with the Li metal as anode and oxygen in the air as cathode active material could achieve a high theoretical energy density of 3500 Wh/kg, which is approximately 10-fold higher than that of LIBs, hoping to replace LIBs as the next generation power batteries for electric vehicles [6–9]. Despite promising, most LABs are still operated in the pure oxygen atmosphere, significantly impeding their practical applications [10,11]. In addition, the extra O_2 gas supply equipment not only greatly deteriorates the energy density of LABs but also complicates the battery system [12,13]. If running in the open air, the early failure of LABs may occur due to the seriously air-induced parasitic reactions, especially on the Li anode side. Moreover, the Li anodes would continuously react with the H_2O, O_2, and CO_2 crossover from the air cathode side to deplete the limited Li reservoir, thus destroying the Li anode/electrolyte interfaces with continuous electrolyte decomposition and increased battery resistance, accelerating the failure of the battery [14,15]. Therefore, it is urgent and necessary to exploit strategies to effectively safeguard the Li anodes of LABs.

At present, approaches including Li anode composition and structure design [3], surface modification with *in/ex-situ* protective films [16–19], and electrolyte composition adjustment (highly concentrated electrolytes [20], Li salts [21], gel or solid-state electrolytes [22,23] and additives [24,25]) have been developed to protect the Li anodes. Among these approaches, the electrolyte engineering [26–28] with simplified experimental steps is a prominent strategy to prevent Li anode from dendrite growth and corrosion

* Corresponding authors.
E-mail addresses: wqliu1979@126.com (W. Liu), ghuang@ciac.ac.cn (G. Huang), xbzhang@ciac.ac.cn (X. Zhang).
[1] These authors contribute equally to this work.

https://doi.org/10.1016/j.cclet.2023.108711
1001-8417/

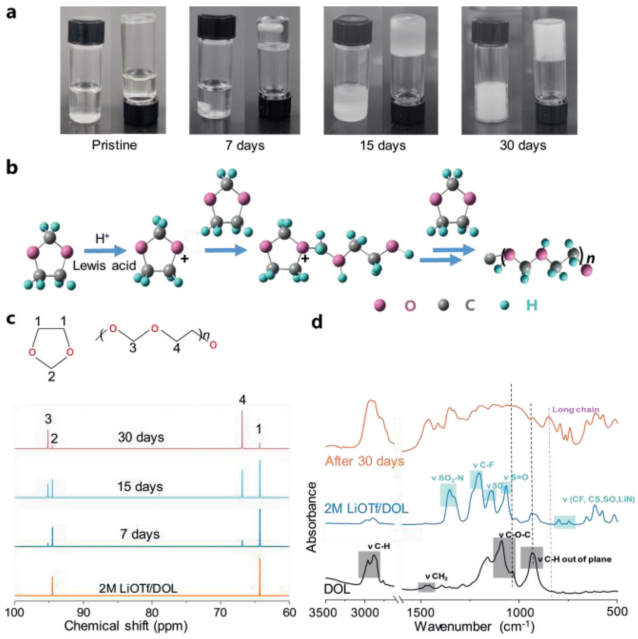

Fig. 1. Polymerization mechanism of the DOL electrolyte. (a) Optical images of the 2 mol/L LiOTf/DOL electrolyte after resting in the air for different times. (b) Schematic of the polymerization process of DOL in the ambient air. (c) ^{13}C NMR spectra of the pristine DOL and poly-DOL at different times. (d) FTIR spectra of the DOL solvent, 2 mol/L LiOTf/DOL electrolyte, and poly-DOL electrolyte.

reactions due to its strong ability to regulate the composition of solid electrolyte interface (SEI) film to facilitate the formation of stable electrode/electrolyte interface [28]. However, the designed electrolytes mainly focus on the Li-O_2 system without consideration of the complex working environment of LABs, in which Li corrosion instead of dendrite growth is the main challenge that limits the long-term operation of battery. To this end, it is paramount to design a suitable electrolyte that could withstand the harsh environment of LABs as well as prompt the formation of a powerful SEI film to effectively protect the Li anodes with air insensitivity.

Herein, an *in-situ* polymerization strategy is crafted by adding 1,3-dioxolane (DOL) into the commonly used tetraethylene glycol dimethyl ether (TEGDME) electrolyte to form a gel polymer electrolyte, in which the DOL could polymerize due to the existence of Lewis acid Li^+ and H_2O in the ambient air. Benefiting from the semi-open nature of LABs, the polymerization of DOL does not need the addition of any electrolyte additives like previous works [29], and a Li^+-conducting gradient protective SEI film is formed on the surface of Li anode to passivate it and block its reaction with the electrolyte and other undesirable components from the air. As a result, the designed gel polymer electrolyte with 1 mol/L $LiCF_3SO_3$ (LiOTf) in DOL/TEGDME (1:1, v/v) successfully prevents the Li anodes from dendrite growth and corrosion reactions, extending the cycle lives of Li/Li symmetrical cells and LABs to 2000 h and 170 cycles, respectively. This gel polymer electrolyte enabled by simply *in-situ* polymerization has displayed unparalleled advantages over other gel polymer electrolytes that gelation with the use of initiator or UV-irradiation, which opens a new avenue for future design of multifunctional SEI films to effectively protect the Li anode to cater the critical demands of LABs.

The optical images in Fig. 1a reveal the gelation process of the 2 mol/L LiOTf/DOL electrolyte in the ambient air. It is clear that this electrolyte gradually changes from the original liquid state to a gel-like solid electrolyte, while the electrolyte in the Ar still keeps the liquid state even after resting for 30 days (Fig. S1 in Supporting informaiton), indicating the air-induced spontaneous polymerization of the DOL electrolyte. Fig. 1b gives the *in-situ* gelation mechanism of DOL. The presence of the strong Lewis acid Li^+ ions and the proton source from H_2O in the air initiates the ring-opening polymerization of DOL. Especially, the exposure of the electrolyte to the air makes its polymerization without the requirements of electrolyte additives, like Al^{3+} [29], Sc^{2+} [30] and Mg^{2+} [31]. To verify the above gelation mechanism, characterizations like nuclear magnetic resonance (NMR) and Fourier transform infrared spectroscopy (FTIR) measurements of 2 mol/L LiOTf/DOL electrolyte at different times were carried out. It can be seen from the NMR spectra of ^{13}C and ^1H (Fig. 1c and Fig. S2 in Supporting informaiton), new hydrogen and carbon peaks appear with gradually increased intensify as prolonging the polymerization time, indicating that the DOL could be polymerized in the ambient air with the existence of Li^+. Meanwhile, the FTIR spectra further confirm this phenomenon (Fig. 1d). Initially, the DOL electrolyte exhibits the C–O-C vibration (1033.5 cm^{-1}) and C–H out of plane vibration (923.3 cm^{-1}) of DOL, but after 30 days of resting, these peaks from the ring of DOL almost disappear, and a new vibration peak (852.3 cm^{-1}) related to the long chain emerges, which is consistent with the previously reported poly-DOL structure [29].

After confirming the air-induced polymerization of the DOL-based electrolyte, this feature could cooperate well with the LABs due its semi-open nature of the cathode side. Then, we investigated the efficacy of the DOL-based gel electrolyte in LABs. Fig. S3 (Supporting informaiton) displays the discharge curves of the LABs with the DOL-based gel electrolyte at 200 mA/g. Only a small discharge capacity of 50 mAh/g could be delivered, which is probably ascribed to the full polymerization of the DOL with limited mobility that results in small three-phase reaction areas and poor contact between the electrolyte and cathode. To resolve this issue, the DOL solvent was added into the TEGDME (G4) electrolyte to prepare 1 mol/L LiOTf/TEGDME-DOL (G4-DOL) to utilize the *in-situ* polymerization feature of DOL while keep the liquid G4 as remnant. As shown in Fig. S4 (Supporting informaiton), like pure DOL electrolyte, after 7-day storage, the liquid G4-DOL electrolyte has also evolved into gel electrolyte but with a certain amount of fluidity, indicating that the polymerization of DOL is not disturbed with the existence of G4. The scanning electron microscope (SEM) images of the separators shows that the polymerized G4-DOL could tightly adheres to the Li anode after cycling, protecting it from corrosion reactions (Fig. S5 in Supporting informaiton).

Then, the reversibility of Li plating/stripping and the stability of Li electrode/electrolyte interface in the designed G4-DOL gel polymer electrolyte were investigated by assembling Li/Li symmetrical cells. As shown in Fig. 2a, the cell with G4 electrolyte possesses a lower polarization in the initial cycles when compared with the cell with G4-DOL, presumably due to the liquid G4 enabled sufficient contact between the Li electrodes and electrolyte. However, obvious overpotential increase can be observed just after 150 cycles (300 h), which is caused by the Li dendrite growth induced continuous electrolyte decomposition with the formation of thicker SEI films and consequently higher interface resistance (Fig. S6 in Supporting informaiton). Thereafter, the continuous accumulation of the uneven Li deposition and Li dendrites makes the short-circuit of G4-based cell with the sudden drop of voltage after 339 h. In contrast, the cell with G4-DOL could stably operate over 2000 h with an almost constant overpotential of around 250 mV (Fig. 2a), which can be vividly reflected in the voltage hysteresis *vs.* cycle number curves in Fig. 2b. This can be attributed to the stable SEI formed by the G4-DOL electrolyte at the Li anode, which promotes smooth plating/stripping of Li while inhibiting dendrite growth. Besides, even at a large current density of 1 mA/cm^2, the cell with G4-DOL still exhibits long-durable lower overpotentials, while the G4-based cell experiences premature death only after 70 cycles (Fig. S7 in Supporting informaiton). To further reveal the in-

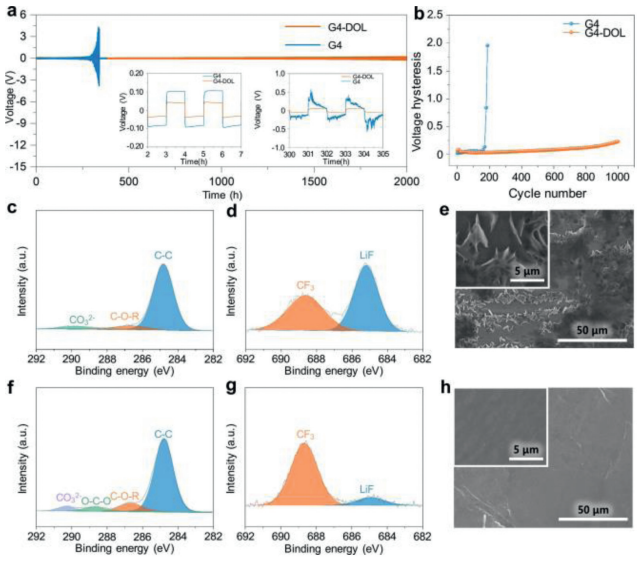

Fig. 2. Electrochemical performance of symmetrical batteries with different electrolytes. (a) Cycling performance of symmetrical Li cells with the G4 and G4-DOL electrolytes at 0.1 mA/cm^2. (b) Voltage hysteresis for Li stripping in Li/Li symmetrical batteries. XPS analyses of (c, f) C 1s and (d, g) F 1s of Li surfaces from symmetrical Li cells with (c, d) G4 and (f, g) G4-DOL electrolytes after 10 cycles. SEM images of Li electrodes from symmetrical Li cells with G4 (e) and G4-DOL (h) electrolytes after 10 cycles.

fluence of the two electrolytes on the Li deposition/dissolution behavior, the impedance evolution of the symmetrical cells was detected. As shown in Fig. S6, the interface impedance gradually increases in the G4-based cell due to the Li dendrite induced poor electrode/electrolyte interfacial stability. For the cell with DOL-G4 electrolyte, there is just a small increase for the interface resistance in the initial cycles, and then it tends to be stable in the following cycling, revealing that the designed DOL-G4 could facilitate uniform Li plating/stripping and stabilize the electrode/electrolyte interface.

To illustrate the anode protection effects of G4-DOL electrolyte, the composition and morphology of the cycled Li anodes were characterized by XPS and SEM. For the Li anode in G4, the C 1s binding energies shows the existences of CO_3^{2-} (290.3 eV) and COOR (286.7 eV), which corresponds to the decomposition of G4 electrolyte (Fig. 2c). The C 1s binding energy for the Li surface in G4-DOL are similar to those of the anode in G4 except with a higher content of organic components due to the existence of polymerized DOL (Fig. 2f). Meanwhile, unlike the dominant LiF (684.9 eV) component in the SEI films formed in the G4 electrolyte (Fig. 2d), the binding energy of CF_3 (688.7 eV) along with much lower LiF prevails in the G4-DOL (Fig. 2g). Furthermore, the typical Li_2S binding energy (163.15 eV) could be detected on the Li anode surface in G4 electrolyte, while it barely exists in the SEI films generated in the G4-DOL (Fig. S8 in Supporting informaiton). After Ar^+ etching for 5 min (Fig. S9 in Supporting informaiton), the LiF content further increases with undetectable CF_3 on the Li anode in G4 electrolyte. For the Li anode in G4-DOL, even with the increased content of LiF in the deeper SEI films, both the LiF and CF_3 still co-exist, which can be attributed to the polymerized DOL that enables more organic components to take part in the formation of SEI films. Consequently, introducing DOL solvent in the G4 electrolyte could help to build a gradient SEI film with the gradual decrease of organic components from top to bottom. The upper layer with rich organic components could behave as a dense layer to prevent the attack from the O_2, H_2O, and CO_2, and thus restricts the occurrence of corrosion reactions. For the bottom LiF-rich layer, it could promote the uniform diffusion of Li^+ with a low barrier and guarantee the firm connection of SEI films with the Li anode [32,33]. Consequently, the cooperation of the organic and LiF-rich layers can not only stabilize the electrode/electrolyte interface but also render dendrite-free plating/stripping of Li. This can be further confirmed by the flat and smooth surface of the Li anode in the G4-DOL (Fig. 2h) and obvious Li dendrite growth on the Li anode in the G4 (Fig. 2e) after 10 cycles.

After proving the effective anode protection function of the designed G4-DOL gel polymer electrolyte, its practical applicability in Li-O_2 batteries (LOBs) and LABs (operated in the air with a relative humidity of 30% ± 2%) were checked. First, the electrochemical stability window of G4-DOL electrolyte was studied. As expected, the G4-DOL exhibits a higher voltage-resistance than G4 (4.56 V *vs.* 4.02 V) due to the passivation effect of polymerization (Fig. S10 in Supporting information). Then, the chemical stability of G4-DOL towards O_2^- and O_2^{2-} was evaluated by NMR. From Figs. S11 and S12 (Supporting information) we can see that there are no new peaks appear after introducing O_2^- and O_2^{2-} species, signifying that the G4-DOL is stable against the reaction intermediates (O_2^- and O_2^{2-}) in LOBs and LABs, which could be attributed to the cross-chain polymerization of the solvent molecules improves the antioxidant of electrolyte. After this, the evolution of discharge products in LOBs was characterized by XRD, FTIR, and SEM. The XRD patterns (Fig. S13 in Supporting information) show that two new peaks at 32.8° and 34.8° corresponding to Li_2O_2 emerge in the discharged cathodes with both G4 and G4-DOL. For FTIR spectra, unlike the clear LiOH signal (3679 cm^{-1}) on the discharged cathode with G4, only Li_2O_2 can be detected with G4-DOL (Fig. S14 in Supporting information), which can be ascribed to the high stability of G4-DOL that avoids the formation of H_2O from the reaction intermediates induced electrolyte decomposition. The morphology of the discharge products in G4-DOL is shown in Fig. S15 (Supporting information). It can be seen that toroidal-type Li_2O_2 particles disperse on the super P cathode and the products disappear after subsequent recharge process, suggesting the G4-DOL could enable the highly reversible formation and decomposition of Li_2O_2. The above results verify that the G4-DOL holds good adaptability in LOBs, which inspires us to extend it to LABs. Figs. 3a and b display the full discharge performance of LOBs and LABs with G4 or G4-DOL at different current densities. No matter in pure oxygen or the ambient air, the cells using G4-DOL always deliver higher discharge capacities and more stable voltage plateaus than those of cells with G4, especially at high current densities. In addition, the rate performance of LOBs and LABs was also evaluated (Figs. 3c and d). In pure O_2 atmosphere, the cell with G4-DOL just exhibits slightly better rate performance than that of the cell with G4 at current densities from 100 mA/g to 1000 mA/g (Fig. 3c). While in the ambient air, the voltage plateaus of the G4-based cell are stable at small current densities, but a much lower and unstable voltage plateau appears when the current density increases to 1000 mA/g (Fig. 3d). Instead, the voltage plateaus with low hysteresis keep stable at all current densities in the G4-DOL-based cell. The G4-DOL rendered excellent rate performance can be attributed to its high electrochemical and chemical stability with limited side reaction products that would impede the fast electron transfer and Li^+ diffusion. Furthermore, the long-term cycling performance of LOBs and LABs was evaluated at 200 mA/g with a limited capacity of 1000 mAh/g. As indicated in Fig. 3e, the LOB with G4-DOL could run for 231 cycles before the discharge terminal voltage drops to 2.0 V, while only 68 cycles are achieved in the cell with G4. Even in the ambient air (Fig. 3f), the G4-DOL-based cell could still realize a durable cycling lifetime (170 cycles), much longer than that of the cell with G4 electrolyte (38 cycles). The reaction atmosphere change resulted lifetime reduction of the G4-DOL-based cell can be ascribed to the complicated discharge products in the cathode side

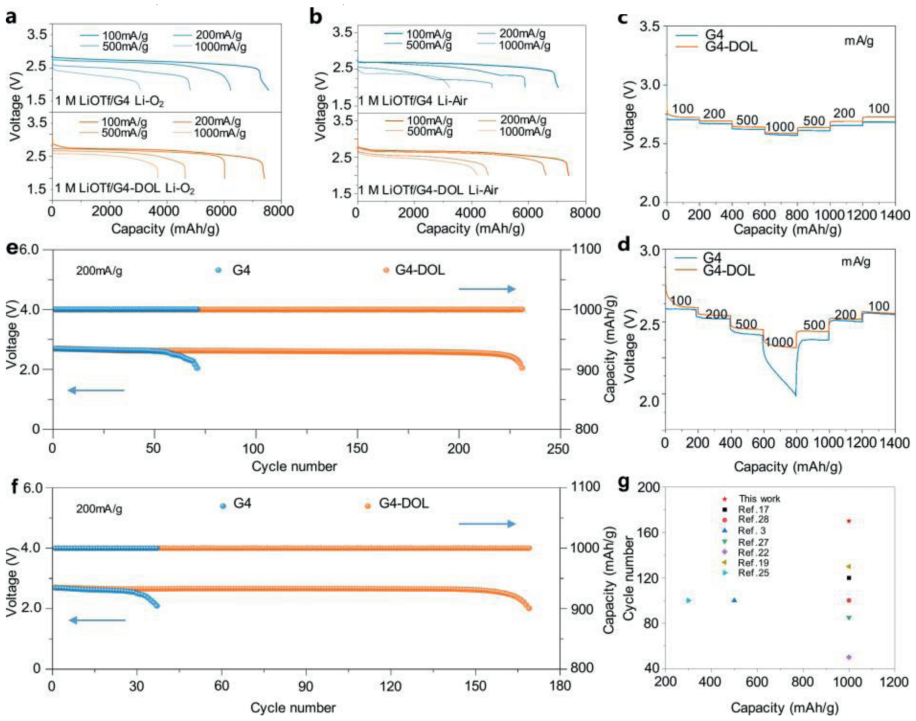

Fig. 3. Electrochemical performance of LOBs and LABs with different electrolytes. Full discharge curves of (a) LOBs and (b) LABs under different current densities. Rate performance of (c) LOBs and (d) LABs at current densities form 100 mA/g to 1000 mA/g. Cycle performance of (e) LABs and (f) LOBs at a specific capacity of 1000 mAh/g. (g) Cycle performance comparison of the LABs.

that involves not only O_2 but also CO_2 and H_2O. The significant performance improvement endowed by the G4-DOL is benefited from its high stability and anode protection ability. Inspiringly, the performance of the LABs acquired with G4-DOL is much superior to the LABs with Li anodes protected by other strategies, like artificial SEI, *ex-situ* gel electrolyte, *etc.* (Fig. 3g).

Then, a question would come in our mind: whether the protective function of G4-DOL on the Li anode still works well in the real working environment of LABs? To answer this, the status of the cycled Li anodes was characterized. Different from the clear LiOH peaks on the anode with G4, no LiOH could be detected on the anode with G4-DOL after 10 cycles (Fig. 4a). When cycling the LABs to 50 cycles, the peaks from Li metal completely disappear in the G4 electrolyte, confirming the severe corrosion of Li anode with continuous loss of active Li. On the contrary, only a weak LiOH peak shows up for the anode in the G4-DOL (Fig. 4b), indicating the effectiveness of G4-DOL in the harsh working environment of LABs on restricting the corrosion of the Li anodes. FTIR and XPS measurements were further conducted to detect the surface components of Li anodes. Fig. S16 (Supporting information) shows a strong LiOH peak (3679 cm^{-1}) on the Li anode after cycling for 10 and 50 cycles in the battery with G4. For the anode in G4-DOL, there is only a small LiOH peak after 10 cycles, and this peak almost remains unchanged even after 50 cycles, suggesting that the gel G4-DOL hinders the air-induced corrosion of Li anode. In addition, Fig. S17 (Supporting information) reveals that the Li surface composes more organic components in the G4-DOL than that in the G4 electrolyte, well maintaining the organic-rich feature of the G4-DOL derived gradient SEI film. Figs. 4c-f give the morphologies of Li anodes after 10 and 50 cycles. Compared with the Li anodes in G4 (Figs. 4c and e), the anodes in G4-DOL exhibit much smoother surfaces with fewer cracks (Figs. 4d and f). Furthermore, the cross-sectional SEM images illustrate that the Li anode in G4 has a corrosion layer of 159 μm in thickness after 10 cycles (Fig. S18 in Supporting information), well consistent with the obvious LiOH

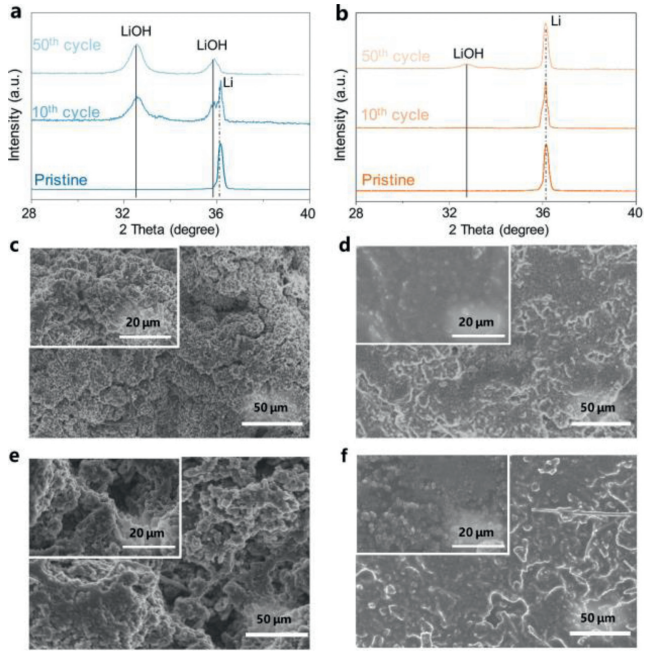

Fig. 4. Surface evolution of the Li anodes after cycling in LABs with different electrolytes. XRD patterns of the Li anodes in LABs with (a) G4 and (b) G4-DOL electrolytes after different cycles. SEM images of the Li anodes in LABs with G4 electrolyte after (c) 10 and (e) 50 cycles. SEM images of the Li anodes in LABs with G4-DOL electrolyte after (d) 10 and (f) 50 cycles.

peaks in the XRD pattern. For the anode in G4-DOL, the thickness of the corrosion layer is only 41 μm, demonstrating the Li corrosion is restrained due to the effective protection ability of the gradient SEI films generated by the G4-DOL. It is worth noting that the LAB paired by the 30th cycled Li anode in G4 with the fresh G4-DOL

could run stably for 45 cycles, while paired with the G4 only realize a lifetime of 5 cycles, again proving the powerful anode protection ability of G4-DOL (Fig. S19 in Supporting information). The enhanced electrochemical performance of the battery with G4-DOL could be mainly attributed to the improved anode stability from the cooperation of the organic and LiF rich layers in the gradient SEI films formed on the surface of Li anodes.

In summary, an *in-situ* formed gel polymer electrolyte (G4-DOL) has been designed by taking full advantage of the semi-open nature of LABs. The formed gel polymer electrolyte could construct a gradient SEI film to effectively prevent the Li anode from dendrite growth and air-induced corrosion reactions, conquering the long-lasting issues that limit the long-term operation of LABs in the ambient air. As a result, the gradient SEI film could facilitate uniform Li plating/stripping and stabilize the electrode/electrolyte interface, significantly prolonging the lifetime of symmetrical Li/Li cells from 340 h to 2000 h. Moreover, when applied the gel polymer electrolyte in LABs, its protective function on Li anode still works well, endowing the batteries with higher discharge capacity, improved rate capability, and also extended lifetime (170 *vs*. 38 cycles in G4 electrolyte). This simple *in-situ* fabrication of gel polymer electrolyte by utilizing the feature of LABs while avoiding the dependence of initiator or UV-irradiation is a powerful way to protect the Li anode to bring LABs closer to practical applications.

Acknowledgments

The authors thank the supports from the National Key R&D Program of China (Nos. 2020YFE0204500 and 2021YFF0500600), National Natural Science Foundation of China (Nos. 52171194 and 52271140), CAS Project for Young Scientists in Basic Research (No. YSBR-058), Youth Innovation Promotion Association of Chinese Academy of Sciences (Nos. 2020230 and 2021223), and Changchun Science and Technology Development Plan Funding Project (No. 21ZY06).

Supplementary materials

Supplementary material associated with this article can be found, in the online version, at doi:10.1016/j.cclet.2023.108711.

References

[1] B. Dunn, H. Kamath, J.M. Tarascon, Science 334 (2011) 928–935.
[2] M. Armand, J.M. Tarascon, Nature 451 (2008) 652–657.
[3] T. Liu, X.L. Feng, X. Jin, et al., Angew. Chem. Int. Ed. 58 (2019) 18240–18245.
[4] Y.S. Tian, G.B. Zeng, A. Rutt, et al., Chem. Rev. 121 (2021) 1623–1669.
[5] D.C. Lin, Y.Y. Liu, Y. Cui, Nat. Nanotechnol. 12 (2017) 194–206.
[6] Y. Yu, X.B. Zhang, Matter 1 (2019) 881–892.
[7] W.J. Kwak, D.Sharon Rosy, et al., Chem. Rev. 120 (2020) 6626–6683.
[8] Z.F. Zhao, Y. Liu, F. Wan, et al., Chin. Chem. Lett. 32 (2021) 594–597.
[9] G.R. Sun, R. Gao, H.L. Jiao, et al., Adv. Mater. 34 (2022) 2201838.
[10] M. Asadi, B. Sayahpour, P. Abbasi, et al., Nature 555 (2018) 502.
[11] H.L. Jiao, G.R. Sun, Y. Wang, et al., Chin. Chem. Lett. 33 (2022) 4008–4012.
[12] G.R. Sun, D.M. Yang, Z.X. Zhang, et al., J. Adv. Ceram. 12 (2023) 747–759.
[13] X.Y. Yang, J.J. Xu, D. Bao, et al., Adv. Mater. 29 (2017) 1700378.
[14] H.K. Lim, H.D. Lim, K.Y. Park, et al., J. Am. Chem. Soc. 135 (2013) 9733–9742.
[15] L. Ye, M. Liao, H. Sun, et al., Angew. Chem. Int. Ed. 58 (2019) 2437–2442.
[16] S. Li, X.S. Wang, Q.D. Li, et al., J. Mater. Chem. A 9 (2021) 7667–7674.
[17] Z. Guo, Q. Zhang, C. Wang, et al., Adv. Funct. Mater. 32 (2021) 2108993.
[18] C. Li, J. Wei, K. Qiu, et al., ACS Appl. Mater. Interfaces 12 (2020) 23010–23016.
[19] X. Zou, K. Liao, D. Wang, et al., Energy Stor. Mater. 27 (2020) 297–306.
[20] H.H. Xu, S.F. Wang, A. Manthiram, Adv. Energy Mater. 8 (2018) 1800813.
[21] Y. Zheng, F.A. Soto, V. Ponce, et al., J. Mater. Chem. A 7 (2019) 25047–25055.
[22] Q.P. Yu, W.C. Mai, W.J. Xue, et al., ACS Appl. Mater. Interfaces 12 (2020) 27087–27094.
[23] H. Kitaura, H.S. Zhou, Energy Environ. Sci. 5 (2012) 9077–9084.
[24] S. Wu, J. Yi, K. Zhu, et al., Adv. Energy Mater. 7 (2017) 1601759.
[25] S.B. Ma, H.J. Kwon, M. Kim, et al., Adv. Energy Mater. 10 (2020) 2001767.
[26] T. Liu, M. Leskes, W.J. Yu, et al., Science 350 (2015) 530–533.
[27] L. Wang, J. Pan, Y. Zhang, et al., Adv. Mater. 30 (2018) 1704378.
[28] Z.Y. Guo, C. Li, J.Y. Liu, et al., Angew. Chem. Int. Ed. 56 (2017) 7505–7509.
[29] Q. Zhao, X. Liu, S. Stalin, et al., Nat. Energy 4 (2019) 365–373.
[30] G.M. Yang, Y.F. Zhai, J.Y. Yao, et al., Chem. Commun. 57 (2021) 7934.
[31] E. Sahadeo, Y. Wang, C.F. Lin, et al., Chem. Commun. 56 (2020) 4583.
[32] Y. Yu, G. Huang, J.Z. Wang, et al., Adv. Mater. 32 (2020) 2004157.
[33] D.W. Sheng, J.H. Zheng, Z.J. Ju, et al., Adv. Mater. 32 (2020) 2000223.